THE JOURNAL OF PHYSICAL CHEMISTRY A

Article

pubs.acs.org/JPCA

Thermal Decomposition Mechanisms of Alkylimidazolium Ionic Liquids with Cyano-Functionalized Anions

Steven D. Chambreau,[†] Adam C. Schenk,[‡] Anna J. Sheppard,[‡] Gregory R. Yandek,[‡] Ghanshyam L. Vaghjiani,*[,‡] John Maciejewski,[§] Christine J. Koh,[∥] Amir Golan,[⊥] and Stephen R. Leone[∥,⊥]

[†]ERC, Inc., and [‡]Propellants Branch, Aerospace Systems Directorate, Air Force Research Laboratory, AFRL/RQRP, Edwards Air Force Base, California 93524, United States

[§]Department of Chemistry, University of Idaho, Moscow, Idaho 83844, United States

[∥]Departments of Chemistry and Physics, University of California, Berkeley, California 94720, United States

[⊥]Lawrence Berkeley National Laboratory, Berkeley, California 94720, United States

Supporting Information

ABSTRACT: Because of the unusually high heats of vaporization of room-temperature ionic liquids (RTILs), volatilization of RTILs through thermal decomposition and vaporization of the decomposition products can be significant. Upon heating of cyano-functionalized anionic RTILs in vacuum, their gaseous products were detected experimentally via tunable vacuum ultraviolet photoionization mass spectrometry performed at the Chemical Dynamics Beamline 9.0.2 at the Advanced Light Source. Experimental evidence for di- and trialkylimidazolium cations and cyano-functionalized anionic RTILs confirms thermal decomposition occurs primarily through two pathways: deprotonation of the cation by the anion and dealkylation of the imidazolium cation by the anion. Secondary reactions include possible cyclization of the cation and C2 substitution on the imidazolium, and their proposed reaction mechanisms are introduced here. Additional evidence supporting these mechanisms was obtained using thermal gravimetric analysis−mass spectrometry, gas chromatography−mass spectrometry, and temperature-jump infrared spectroscopy. In order to predict the overall thermal stability in these ionic liquids, the ability to accurately calculate both the basicity of the anions and their nucleophilicity in the ionic liquid is critical. Both gas phase and condensed phase (generic ionic liquid (GIL) model) density functional theory calculations support the decomposition mechanisms, and the GIL model could provide a highly accurate means to determine thermal stabilities for ionic liquids in general.

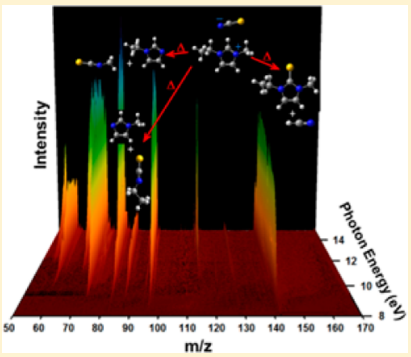

I. INTRODUCTION

Ionic liquids (with mp ≤ 100 °C) consist of discrete ions and have distinctly different physical and chemical properties from molecular liquids.[1] The most widely recognized characteristic of ionic liquids is their negligible vapor pressure, making them attractive candidates for replacements of volatile organic compounds commonly used as reaction solvents.[2] In order to depress the melting point of ionic solids, it is necessary to reduce the Coulombic attraction between cations and anions. This can be achieved through functionalization of small, tightly bound ions to create larger, more diffusely charged ions. Often, the reduction in Coulombic attraction between the ions results in glass formation rather than actual melting of the solid. In the successful synthesis of ionic liquids, their viscosities tend to remain unusually high, which can limit their usefulness as solvents.

The dicyanamide anion-based family of room-temperature ionic liquids (RTILs) exhibits some of the lowest viscosities of any known RTILs.[3] They can be easily prepared from the appropriate halide salts and silver dicyanamide and were the first RTILs to demonstrate hypergolic reactivity (spontaneous ignition) when mixed with white fuming nitric acid.[3,4] Ionic liquids are not only well-known for their negligible vapor pressures but also for their thermal stability. Because of their extremely low affinity for protons, bis(trifluoromethylsulfonyl)-imide (Tf_2N^-) based RTILs are known to be highly thermally stable.[5−7] Significant theoretical work has been done on RTILs in the gas phase and by force field methods and quantum mechanics/molecular mechanics (QM/MM).[8−12] However, predicting reaction energetics in the condensed phase is difficult due to the ionic nature of the solvent; the solvent effects on the relative stabilities of the reactants, transition states, and products involved in the reaction will affect both the rate and free energy of reaction.[13] The development and implementation of an accurate yet efficient theoretical approach to investigate the condensed phase reaction energetics of ionic liquids is highly desirable. Recent work in this regard using the conductor-type polarizable continuum model (CPCM),[14] an ab

Received: September 22, 2014
Revised: November 3, 2014
Published: November 10, 2014

 © 2014 American Chemical Society dx.doi.org/10.1021/jp5095855 | J. Phys. Chem. A 2014, 118, 11119−11132

initio method to simulate condensed phase conditions, shows great promise in this application.[13,15]

In this article, we investigate the thermal stability of RTILs with cyano-functionalized anions such as dicyanamide ($(CN)_2N^-$), thiocyanate (SCN^-), tricyanomethanide ($(CN)_3C^-$), and vinylogous dicyanamide ($(CN)_2C{=}CHNCN^-$) using a combination of several experimental probes and theory. Thermal gravimetric analysis (TGA) yields enthalpy of vaporization (isothermal) and overall activation enthalpy of thermal decomposition (nonisothermal), and when coupled with electron-impact ionization mass spectrometry (TGA–MS), the activation enthalpies for individual thermal decomposition pathways of the ionic liquid can be obtained. Identification of vaporized products is also confirmed using gas chromatography–mass spectrometry (GC–MS) and temperature-jump (T-jump) FTIR techniques. Finally, tunable vacuum ultraviolet photoionization time-of-flight mass spectrometry (VUV–PI–TOFMS) is used to identify the masses and ionization potentials of the gas-phase species evolved above a heated RTIL in a vacuum. The trends in these results have led to improved predictive capabilities using density functional theory (DFT) applied to the generic ionic liquid model (GIL), and direct dynamics modeling (see companion article[16]) that should be applicable to predicting thermal stabilities of other RTILs.

II. EXPERIMENTAL SECTION

1-Butyl-3-methylimidazolium tricyanomethanide ($BMIM^+TCM^-$, >98% purity) and 1-butyl-3-methylimidazolium dicyanamide ($BMIM^+DCA^-$, >99% purity) were purchased from Merck and used without further purification. 1-Ethyl-3-methylimidazolium dicyanamide ($EMIM^+DCA^-$ ≥98.5% purity), 1-ethylimidazolium thiocyanate ($EMIM^+SCN^-$, ≥99% purity), and 1-butyl-3-methylimidazolium thiocyanate ($BMIM^+SCN^-$, ≥95% purity) were purchased from Fluka and used without further purification. 1-Butyl-3-methylimidazolium vinylogous dicyanamide ($BMIM^+VDCA^-$) was synthesized as described.[17] 1-Ethyl-2,3-dimethylimidazolium dicyanamide ($EMMIM^+DCA^-$) was synthesized according to the procedure in ref 1.

The T-jump experiment[18,19] was carried out on a rapid scan FTIR spectrometer with 4 cm^{-1} resolution and 10 ms time resolution between spectra. An ionic liquid sample of about 3 μL was placed on a nichrome filament, and the vapor phase above the filament was analyzed by FTIR spectroscopy after a 1F capacitor discharged approximately 17 V across the nichrome ribbon, reaching maximum temperature in ∼50 ms. The discharge of the capacitor triggered the FTIR spectrometer. The experiment was conducted with an initial temperature of 298 K and at 1 atm pressure. Maximum temperatures recorded for the ILs are as follows: $BMIM^+SCN^-$ T_{max} = 461 K, $BMIM^+DCA^-$ T_{max} = 684 K, and $BMIM^+TCM^-$ T_{max} = 675 K.

The TGA and TGA–MS experiments were similar to those described previously.[20,21] Briefly, the nonisothermal TGA measurements were carried out with a temperature ramp rate of 10 K/min from 303 to 973 K, and the isothermal TGA measurements typically were carried out from 423 to 573 K in either 5 or 10 K steps with a 30 min hold time at each step. Ionization in the TGA–MS experiments was achieved by electron impact ionization (70 eV).

GC–MS analysis was run with the electron impact ionizer tuned to 15 eV. VUV–PI–TOFMS experiments included the improved effusive ionic liquid source[21] and the aerosol source[22] described previously. Briefly, the RTILs were introduced into the sources where they were heated and the vapor coming of the heated RTIL was probed as a function of heater temperature and VUV photon energy. For both the TGA–MS and VUV–PI–TOFMS experiments, no ions were detected above m/z = 200 amu.

III. THEORY

Hybrid density functional theory was applied at the M06/6-31+G(d,p) level of theory[23] to investigate these IL systems. M05 has been shown to provide a good level of theory for calculating energetics of ionic liquid systems (mean average deviation, MAD, of 9.5 kJ/mol),[24] and M06 is presumed to be as good if not better than M05 for our purposes. Stationary states of reactants, intermediates, transition states, and products, as well as adiabatic photoionization potentials were calculated using Gaussian 09.[25] Transition states were confirmed to have a single imaginary frequency and through intrinsic reaction coordinate analysis.

A variant of the quantum mechanical continuum solvation model SMD[26] known as the generic ionic liquid (SMD-GIL) model[15] was employed to calculate free energies in the ionic liquid condensed phase. The SMD-GIL solvent descriptor input parameters used for $EMIM^+DCA^-$ as a solvent are e = 11.50, n = 1.4300, γ = 61.24, $\Sigma\alpha_2^H$ = 0.229, $\Sigma\beta_2^H$ = 0.265, φ = 0.2308, and ψ = 0.0000,[15] while φ = 0.2727 and 0.200 for $EMIM^+SCN^-$ and $EMIM^+TCM^-$, respectively. The fraction of non-hydrogen atoms that are electronegative halogen atoms (ψ) is zero for DCA^-, SCN^-, TCM^-, and $VDCA^-$ containing ionic liquids and ψ = 0.0500 for $EMIM^+Br^-$. SMD-GIL calculations were carried out using M06/6-31+G(d,p) in Gaussian 09.[25]

IV. RESULTS

The thermal decomposition of cyano-functionalized anionic RTILs was investigated using several complementary experimental probes, including TGA, TGA–MS, temperature-jump FTIR spectroscopy, GC–MS, and VUV–PI–TOFMS. For brevity, a representative spectrum from each experimental technique will be presented here, and the remainder of the data, along with thermal decomposition reaction schemes for each ionic liquid, can be found in the Supporting Information. Numeric data is summarized in Tables 1–5.

A. Thermal Gravimetric Analysis. Thermal gravimetric analysis (TGA) is a measurement of the mass of a sample as it is heated, typically with an inert gas flowing over the sample. In an inert environment, the mass loss as the temperature increases can be the result of both vaporization of the sample and of the thermal decomposition of the sample followed by subsequent vaporization of the thermal decomposition products. For volatile species (having small enthalpies of vaporization, ΔH_{vap}), simple evaporation takes place and 100% of the sample mass is lost due to vaporization of the intact species. The rate of evaporation is dependent on the enthalpy of vaporization (ΔH_{vap}) of the species, the surface area of the sample, and the flow and molecular mass of inert gas over the sample.[6,27] Conversely, for easily decomposing species typically having high ΔH_{vap}, first decomposition must occur and the products must diffuse to the surface of the sample, where they can evaporate. Mass loss due to thermal decomposition processes can be less than 100% if thermal decomposition products have low volatility or form solids. The rate of thermal

dx.doi.org/10.1021/jp5095855 | J. Phys. Chem. A 2014, 118, 11119–11132

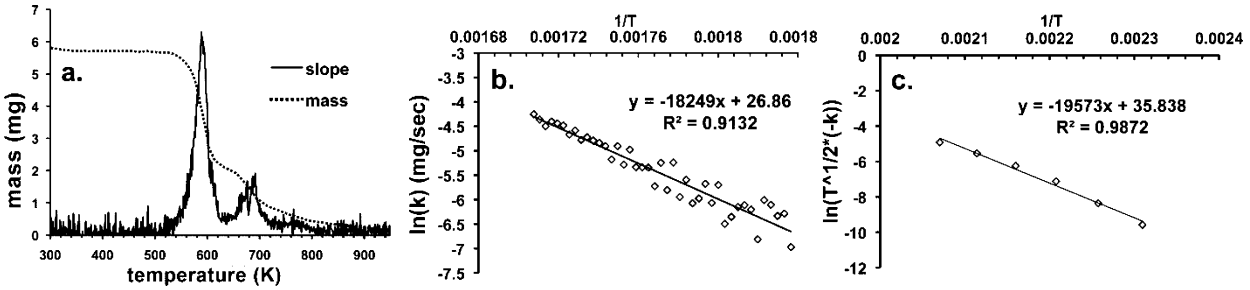

Figure 1. Thermal gravimetric analysis of 1-ethyl-3-methylimidazolium dicyanamide: (a) TGA, (b) Arrhenius plot of slope from panel a, (c) isothermal TGA to determine ΔH_{vap} = 140.9 ± 19.2 kJ/mol (298 K).

Table 1. Experimental Enthalpies of Activation, $\Delta H^{\ddagger}$(overall), and Vaporization, ΔH_{vap} (at T_{avg} and 298 K) Determined by TGA; Enthalpies Are in kJ/mol, $\Delta_l^g C_{pm}^o$ Is in J/mol·K, and Temperatures Are in K

ionic liquid	$\Delta H^{\ddagger}$(overall)	T_{avg}	ΔH_{vap}	T_{avg}	$\Delta_l^g C_{pm}^o$	ΔH_{vap}(298)
$EMIM^+DCA^-$	151.7 ± 14.5	566	128.3 ± 19.2	473	−72.0[a] ± 3.3	140.9 ± 19.2
$BMIM^+DCA^-$	159.5 ± 10.2	560	133.1 ± 5.0	488	−72.5[a] ± 3.3	146.9 ± 5.0
$EMMIM^+DCA^-$	268.4 ± 50.9	618	185.2 ± 14.2	513	−70[d]	200.3 ± 14.2
$EMIM^+SCN^-$	118.0 ± 3.7	535	150.7 ± 10.8	458	−60.8[b] ± 2.8	160.4 ± 10.8
$BMIM^+SCN^-$	165.7 ± 5.0	517	168.6 ± 9.2	448	−70.6[b] ± 3.2	179.9 ± 9.2
$BMIM^+TCM^-$[21]	183.0 ± 4.3	582	126.0 ± 6.2	473	−78.9[c] ± 3.6	139.8 ± 6.2
$BMIM^+VDCA^-$	105.1 ± 25.3	475	62.1 ± 25.3	453	−70[d]	73.0 ± 25.3

[a]Reference 31. [b]Reference 32. [c]References 33 and 34. [d]Estimated value, see text for details.

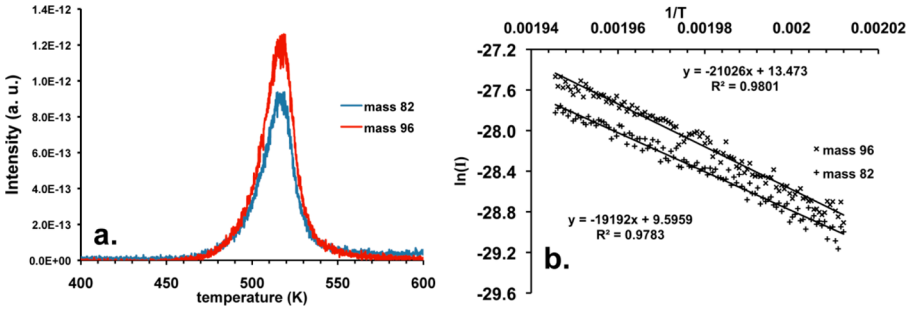

Figure 2. (a) TGA−MS analysis of $EMIM^+DCA^-$: mass 82 (methylimidazole) and 96 (ethylimidazole) and (b) Arrhenius plot of data from panel a: $\Delta H^{\ddagger}_{96}$ = 159.6 ± 2.3 kJ/mol (505 K) and $\Delta H^{\ddagger}_{82}$ = 174.8 ± 2.4 kJ/mol (505 K).

decomposition depends on the overall activation enthalpies, $\Delta H^{\ddagger}$(overall), for all decomposition pathways and is not dependent upon surface area of the sample.[6,27] The total mass loss rate by TGA is the sum of the mass loss from evaporation and the mass losses from all thermal decomposition processes, which produce volatile species. However, because the evaporation and thermal decomposition rates are dependent on different factors, the vaporization rates for low-volatility species such as RTILs can be accurately determined by an isothermal analysis[28] and the thermal decomposition rates are better measured by fast heating rates.[6] When the enthalpy of vaporization (ΔH_{vap}) is comparable to or higher than the overall activation enthalpy $\Delta H^{\ddagger}$(overall) for thermal decomposition, then mass loss by thermal decomposition competes with or dominates over mass loss by evaporation.[20,29,30] Enthalpies of vaporization of RTILs range from 120 kJ/mol to over 200 kJ/mol, and thermal decomposition is a highly competitive process in these compounds.

The TGA of 1-ethyl-3-methylimidazolium dicyanamide, $EMIM^+DCA^-$, indicates a mass loss onset (nonzero slope) temperature above 510 K with two distinct peaks at 590 and 690 K (Figure 1a). Fitting the lowest temperature peak in an Arrhenius plot (Figure 1b), where the slope of $\ln(k)$ versus $1/T$ equals $-\Delta H^{\ddagger}$(overall)/R, yields an enthalpy for the overall mass loss rate of $\Delta H^{\ddagger}$(overall) = 151.7 ± 14.5 kJ/mol (±95% confidence limits) at an average temperature (T_{avg}) of 566 K (Table 1). In order to determine the enthalpy of vaporization (ΔH_{vap}) of $EMIM^+DCA^-$, isothermal TGA analysis (described previously),[21,28] where the slope of $\ln [T^{1/2}(dm/dt)]$ versus $1/T$ equals $\Delta H_{vap}/R$ (Figure 1c), yields a ΔH_{vap} value of 128.3 ± 19.2 kJ/mol (T_{avg} = 473 K, determined to be the average temperature in Figure 1c), which when corrected to 298 K using $\Delta_l^g C_{pm}^o$ (the change in molar heat capacity from liquid to the gas phase) of −72.0 J/K (see Table 1 and discussion for details)[10] gives ΔH_{vap}(298) = 140.9 ± 19.2 kJ/mol.

For $EMIM^+DCA^-$ and several other cyano-functionalized anionic RTILs, there are several peaks in the TGA and the mass loss does not reach 100% at high temperature. This indicates that there are several different thermal decomposition processes occurring in different temperature regimes and that some solid is formed that is not volatile. Previous work on dicyanamide-based ionic liquids indicates that the dicyanamide anion can polymerize when heated,[35] perhaps through a melamine intermediate.[36,37] This will be discussed in more detail in the discussion section.

dx.doi.org/10.1021/jp5095855 | J. Phys. Chem. A 2014, 118, 11119−11132

B. Thermal Gravimetric Analysis–Mass Spectrometry. A powerful enhancement to standard TGA is to couple the TGA to a mass spectrometer via a heated capillary tube (433 K). Volatile neutral species evolved from the TGA are ionized by electron impact ionization (70 eV) and can then be identified by their mass-to-charge ratios (m/z), and their fragmentation patterns, although fragmentation in the TGA–MS is extensive and therefore complex, will not be discussed here. Furthermore, by monitoring a product species parent mass as a function of temperature, the activation enthalpy for its formation can be calculated using an Arrhenius-type analysis. The major species detected by TGA–MS analysis of $EMIM^+DCA^-$ are m/z = 82 and 96 (Figure 2a), and an Arrhenius plot for these masses (Figure 2b) yields the activation enthalpies for their formation, $\Delta H^{\ddagger}_{96}$ = 160 ± 16 kJ/mol and $\Delta H^{\ddagger}_{82}$ = 175 ± 17 kJ/mol at T_{avg} = 505 K. A conservative estimate of ±10% was assigned to the uncertainties in $\Delta H^{\ddagger}$ due to possible systematic errors arising from mass transport (related to the chemical's vapor pressure) differences between the TGA and the mass spectrometer and ion transmission efficiency differences in the mass spectrometer itself. $\Delta H^{\ddagger}$ values calculated for selected masses of all ionic liquids are seen in Table 2.

Table 2. Experimental Enthalpies of Activation, $\Delta H^{\ddagger}$, for Individual Masses (at T_{avg}) Determined by TGA–MS Analysis; Enthalpies Are in kJ/mol, m/z Values Are in amu, and Temperatures Are in K; Uncertainties Are Estimated to be ±10%

ionic liquid	$\Delta H^{\ddagger}$	m/z	$\Delta H^{\ddagger}$	m/z	T_{avg}
$EMIM^+DCA^-$	160 ± 16	96	175 ± 17	82	505
$BMIM^+DCA^-$	150 ± 15	82	162 ± 16	97	510
$EMMIM^+DCA^-$	140 ± 14	96	137 ± 14	110	530
$BMIM^+TCM^-$	128 ± 13	78	98 ± 10	82	525
$EMIM^+SCN^-$	128 ± 13	73	109 ± 11	82	478
	126 ± 13	87	110 ± 11	96	478

C. Vacuum Ultraviolet Photoionization–Time of Flight Mass Spectrometry. Representative vacuum ultraviolet time-of-flight mass spectrometry (VUV–TOFMS) data for $EMIM^+DCA^-$ can be seen in Figure 3. Figure 3a shows a contour plot of the photoion intensities with a VUV photon energy range of 7.4–10.0 eV at an effusive source temperature of T = 473 K, and Figure 3b is the corresponding photoionization mass spectrum at 9.0 eV. Photoionization efficiency (PIE) curves for masses 82, 96, 110, and 150 are seen in Figure 3c,d, and the total ion intensities (sum over all photon energies) of these masses are plotted as a function of effusive source temperature in Figure 3e. Photoion appearance energies were determined for the major photoions by fitting the PIE curves to the function $\alpha(E - E_o)^2$ near the photoionization threshold, as described previously,[9,22,38] and are reported along with their calculated (M06/6-31+G(d,p), 298 K) adiabatic ionization energies and relative ion abundances in Table 3.

Investigation by VUV–PI–TOFMS for 1-butyl-3-methylimidazolium dicyanamide ($BMIM^+DCA^-$) was extensively performed for this species. Figure 4a–c represents two VUV–TOFMS spectra that are generated by low temperature evaporation of $BMIM^+DCA^-$ aerosols as described previously[22] (Figures 4a,b, 380 K), or by the effusive ionic liquid source at 483 K and photoionized at 10.0 eV (Figure 4c). Figure 4d is from GC–MS analysis of $BMIM^+DCA^-$ with a 15 eV electron-impact ionization source, indicating a parent ion mass of m/z = 178. In Figure 5, the scaled mass spectra indicate the changes in the $BMIM^+$ cation signal as a function of temperature in the range of 438–483 K photoionized at 12.0 eV and averaged over 5 million repeller pulses.

D. Temperature-Jump Fourier Transform Infrared Spectroscopy. Likely because of polymerization, no coproducts containing the DCA^- or TCM^- anions were observed using the TGA–MS or the effusive source in the VUV experiments. Therefore, temperature-jump Fourier transform infrared spectroscopy (T-jump FTIR) was employed in an attempt to rapidly vaporize the products before they could polymerize. The experimental design is based on previous work by Brill and co-workers.[18,19] Gas phase T-jump FTIR spectroscopy results for $BMIM^+SCN^-$, $BMIM^+TCM^-$, and $BMIM^+DCA^-$ are seen in Figure 6.

V. DISCUSSION

A. Thermal Gravimetric Analysis. In comparing the TGA data for all of the investigated CN-containing anionic ionic liquids, the only ILs to achieve near 100% mass loss are the thiocyanates 1-ethyl-3-methylimidazilium thiocyanate, $EMIM^+SCN^-$, and 1-butyl-3-methylimidazolium thiocyanate, $BMIM^+SCN^-$. All of the other ILs investigated have mass losses <100%, indicating solid residue formation, likely through polymerization of the anions or their thermal decomposition products.[35,36] This indicates that the thermal decomposition products in the SCN^- systems either do not easily polymerize or are able to vaporize before polymerization can occur. From Table 1, based on the overall $\Delta H^{\ddagger}$ values, the trend in stability, from least to most stable is $BMIM^+VDCA^- < EMIM^+SCN^- < EMIM^+DCA^- < BMIM^+DCA^- < BMIM^+SCN^- < BMIM^+TCM^- < EMMIM^+DCA^-$. Similarly, from Table 1, based on the overall ΔH_{vap} values, the trend in enthalpies of vaporization, from lowest to highest, is $BMIM^+VDCA^- < BMIM^+TCM^- < EMIM^+DCA^- < BMIM^+DCA^- < EMIM^+SCN^- < BMIM^+SCN^- < EMMIM^+DCA^-$, which is consistent with previous experimental and theoretical heats of vaporization for these ILs.[7,10,41–45] The heat of vaporization determined for $BMIM^+VDCA^-$ is unusually low (Table 1) and is likely attributable to mass loss from thermal decomposition instead of from vaporization of the intact IL. If this is true, then based on enthalpies of vaporization, the most volatile IL is $BMIM^+TCM^-$. This species has been detected directly in the vapor phase and has one of the highest vapor pressures of known ILs.[21,46] Clearly, for the thiocyanate ILs, since their overall activation enthalpies determined by TGA are significantly lower than their enthalpies of vaporization, thermal decomposition is strongly favored over vaporization at moderate temperatures (T < 573 K) in these ILs, as has been observed previously for dialkylimidazolium carboxylate ionic liquids.[13] Conversely, for the tricyanomethanide and trialkylimidizolium dicyanamide ILs, their enthalpies of vaporization are significantly lower than their overall thermal decomposition activation enthalpies, and vaporization is favored over thermal decomposition at moderate temperatures (T < 573 K). For the dialkylimidazolium dicyanamides, where their overall thermal decomposition activation enthalpies and enthalpies of vaporization are fairly similar, it is likely that thermal decomposition and vaporization are competing below T = 573 K. It is important to note that, according to Trouton's Rule ($\Delta S_{vap} \approx 10.5R$),[47] entropic contributions are typically larger for vaporization than for thermal decomposition

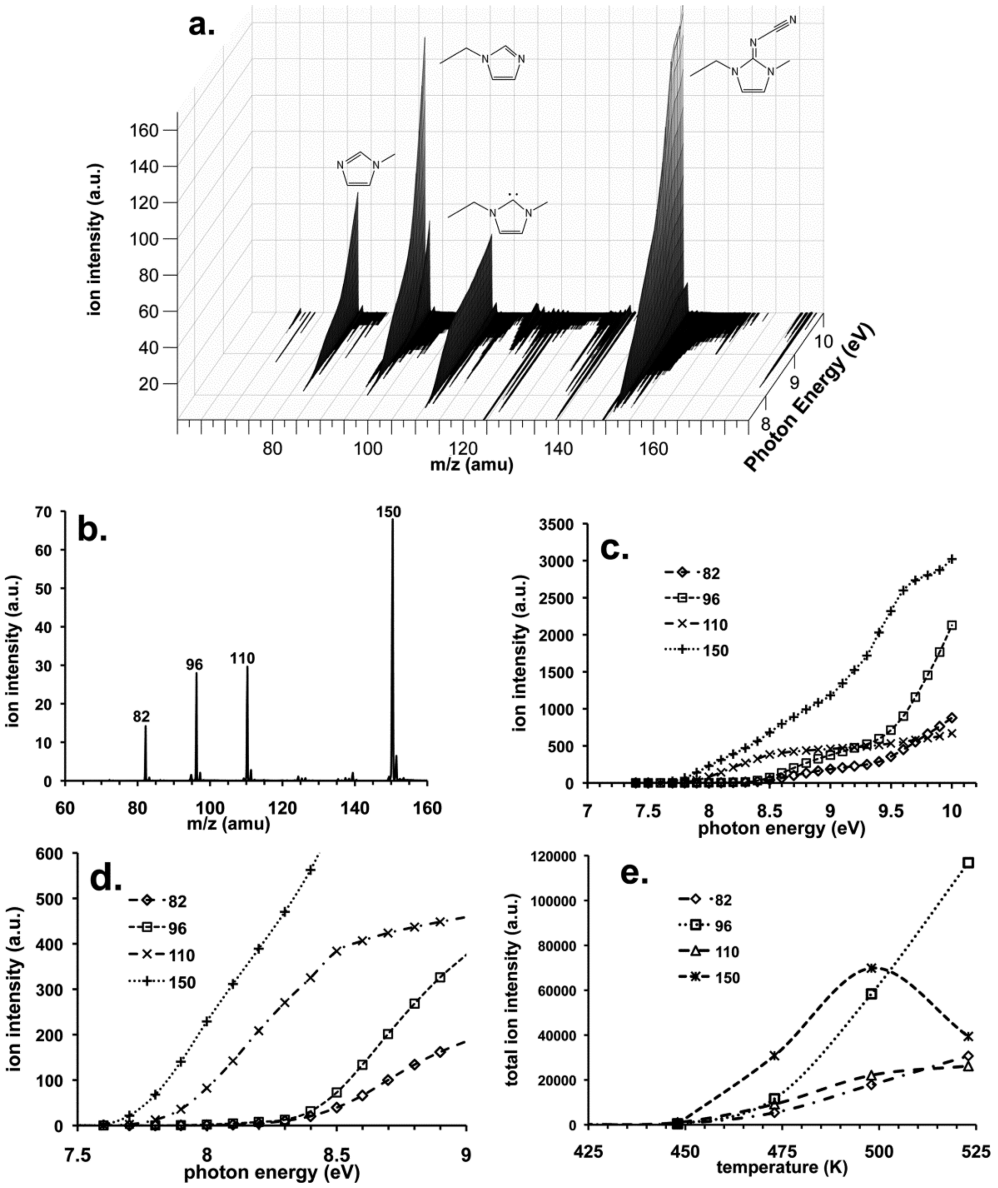

Figure 3. (a) VUV−PI−TOFMS analysis of $EMIM^+DCA^-$ at 473 K from 7.4 to 10.0 eV photon energy and (b) 9.0 eV photon energy, (c) PIE curves for masses in panel b, (d) expanded view of the photoion thresholds from panel c, and (e) total ion count/relative abundance of the photoions from 450 to 525 K.

processes in the condensed phase discussed here ($\Delta S < 4R$), and this effectively lowers the free energy of vaporization more than for thermal decomposition versus considering only the enthalpies in these two competing processes.

In order to accurately determine the enthalpy of vaporization of ionic liquids under standard conditions (298 K), it is important to accurately determine $\Delta_l^g C_{pm}^o$, the change in molar heat capacity from liquid to the gas phase.[7,43,45,48−50] A recent study by Verevkin[10] and co-workers have demonstrated that $\Delta_l^g C_{pm}^o$ can be estimated by

$$\Delta_l^g C_{pm}^o = -2R - (C_{pm}^o - C_{vm}^o)_l \quad (1)$$

where:

$$(C_{pm}^o - C_{vm}^o)_l = \frac{\alpha_p^{\,2}}{K_T} V_m T \quad (2)$$

and α_p is the thermal expansion coefficient, K_T is the isothermal compressibility, and V_m is the molar volume of the ionic liquid. Prior to this work, $\Delta_l^g C_{pm}^o$ values were simply estimated to be 100 J/mol·K, and this assumption was the main source of error in measuring standard enthalpies of vaporization of ionic liquids. For this work, literature values for α_p and K_T for five of the ionic liquids were used to calculate the $\Delta_l^g C_{pm}^o$ values in Table 1. The 100 J/mol·K value for $\Delta_l^g C_{pm}^o$ used previously was based on much work with the bis(trifluoromethanesulfonyl)-imide anion-based ionic liquids, which have large molar heat capacities (500−1000 J/mol·K at 298 K[10]). The ionic liquids investigated here have smaller molar heat capacities (~300 J/mol·K) and would be expected to have smaller $\Delta_l^g C_{pm}^o$ values as well. In fact, the $\Delta_l^g C_{pm}^o$ values in Table 1 average about 70 J/mol·K, and this value was used as an estimate for $\Delta_l^g C_{pm}^o$ for $EMMIM^+DCA^-$ and for $BMIM^+VDCA^-$, where no α_p or K_T values were available. This more accurate value for $\Delta_l^g C_{pm}^o$ decreases the standard enthalpies of vaporization for these ionic

dx.doi.org/10.1021/jp5095855 | J. Phys. Chem. A 2014, 118, 11119−11132

Table 3. VUV−TOFMS Data for All Ionic Liquids Investigated; ΔG_{298} Values Are in eV

EMIM$^+$DCA$^-$, 463 K			
mass (amu)	appearance energy (eV)	ΔG_{298} M06/6-31+G (d,p)	relative abundance (%)
27	13.4 ± 0.2	13.3 ± 0.2	4.4
82	8.3 ± 0.2	8.4 ± 0.2	14.2
96	8.3 ± 0.2	8.3 ± 0.2	23.9
110	7.6 ± 0.2	7.7 ± 0.2	11.4
150	7.5 ± 0.2	7.6 ± 0.2	45.3
EMIM$^+$DCA$^-$, 483 K			
mass (amu)	appearance energy (eV)	ΔG_{298} M06/6-31+G (d,p)	relative abundance (%)
27	13.4 ± 0.2	13.3 ± 0.2	4.0
82	8.4 ± 0.2	8.4 ± 0.2	20.5
97	7.6 ± 0.2	ND	18.0
124	8.2 ± 0.2	8.3 ± 0.2	15.6
137	7.9 ± 0.2	ND	15.1
178	7.6 ± 0.2	8.3 ± 0.2	5.4
EMIM$^+$DCA$^-$, 423 K			
mass (amu)	appearance energy (eV)	ΔG_{298} M06/6-31+G (d,p)	relative abundance (%)
96	7.7 ± 0.2	8.0 ± 0.2	17.0
110	7.9 ± 0.2	7.9 ± 0.2	6.1
124	6.0 ± 0.5	6.1 ± 0.2	52.8
125	7.2 ± 0.5	7.2 ± 0.2	23.9
EMIM$^+$SCN$^-$, 467 K			
mass (amu)	appearance energy (eV)	ΔG_{298} M06/6-31+G (d,p)	relative abundance (%)
27	13.3 ± 0.2	13.3 ± 0.2	3.4
73	8.2 ± 0.2	9.1 ± 0.2 (CH_3NCS)	23.2
82	8.4 ± 0.2	8.4 ± 0.2	8.8
87	9.1 ± 0.2	9.0 ± 0.2 (CH_3CH_2NCS)	4.6
96	8.3 ± 0.2	8.3 ± 0.2	30.9
EMIM$^+$SCN$^-$, 467 K			
mass (amu)	appearance energy (eV)	ΔG_{298} M06/6-31+G (d,p)	relative abundance (%)
142	7.1 ± 0.3	7.2 ± 0.2	29.1
EMIM$^+$SCN$^-$, 493 K			
mass (amu)	appearance energy (eV)	ΔG_{298} M06/6-31+G (d,p)	relative abundance (%)
27	13.4 ± 0.2	13.3 ± 0.2	4.4
73	9.1 ± 0.2	9.1 ± 0.2 (CH_3NCS)	29.3
82	8.3 ± 0.2	8.4 ± 0.2	19.7
97	9.3 ± 0.2	ND	9.3
124	8.1 ± 0.2	8.3 ± 0.2	15.1
137	9.2 ± 0.2	ND	20.3
171	8.8 ± 0.2	7.1 ± 0.2	1.8
EMIM$^+$TCM$^-$, 433 K			
mass (amu)	appearance energy (eV)	ΔG_{298} M06/6-31+G (d,p)	relative abundance (%)
82	8.2 ± 0.2	8.4 ± 0.2	1.1
96	7.6 ± 0.2	ND	67.9
110	7.7 ± 0.2	ND	2.0
124	8.2 ± 0.2	8.3 ± 0.2	4.6
137	7.6 ± 0.2	ND	17.8
139	7.1 ± 0.3	6.9 ± 0.2	3.4
229	6.6 ± 0.5	7.3 ± 0.2	3.1
EMIM$^+$VDCA$^-$, 413 K			
mass (amu)	appearance energy (eV)	ΔG_{298} M06/6-31+G (d,p)	relative abundance (%)
96	7.7 ± 0.2	ND	1.2
110	8.0 ± 0.2	ND	8.0
124	8.2 ± 0.2	8.3 ± 0.2	2.1
137	7.6 ± 0.2	ND	8.0
178	7.1 ± 0.3	8.3 ± 0.2	43.6

liquids by an average of 5.1 kJ/mol relative to those using the $\Delta^g_l C^o_{pm} = -100$ J/mol·K value.

B. Thermal Gravimetric Analysis Mass Spectrometry. Since the TGA results do not discriminate between vaporization and the thermal decomposition pathways available, TGA−MS is better suited for analyzing specific reaction pathways by monitoring volatile thermal decomposition products as a function of temperature; vaporization of ILs is not likely to be detected, as the ILs will condense in the capillary coupling the TGA to the mass spectrometer. Major mass peaks that were detected are listed in Table 2 along with their activation enthalpies of formation, which were calculated using an Arrhenius type analysis on the low temperature regime of the TGA−MS plots in Figure 2a and in the Supporting Information. Because of the high energy of electron impact ionization used in the TGA−MS (70 eV), extensive fragmentation of the ionized products occurs, and only products with masses above 70 amu were considered in the TGA−MS experiments. Fragmentation using "soft" tunable vacuum ultraviolet photoionization is minimized and is much simpler to interpret, and will be discussed in detail in the next section.

TGA−MS results for the thermally unstable BMIM$^+$VDCA$^-$ were complex and difficult to interpret, likely due to multiple decomposition pathways, and will not be discussed here. The next most sensitive IL to thermal decomposition, EMIM$^+$SCN$^-$, evolves masses at m/z 73, 82, 87, and 96 with activation enthalpies of (T_{avg} = 478 K) $\Delta H^{\ddagger}_{73}$ = 128 ± 13 kJ/mol, $\Delta H^{\ddagger}_{82}$ = 109 ± 11 kJ/mol, $\Delta H^{\ddagger}_{87}$ = 126 ± 13 kJ/mol, and $\Delta H^{\ddagger}_{96}$ = 110 ± 11 kJ/mol (uncertainty estimated at 10%), respectively, and a small signal at m/z 142, which was too small to determine the thermal decomposition activation enthalpy. Mass at m/z 27 was difficult to detect due to interference from the large m/z 28 N_2 carrier gas signal. Note that these activation enthalpies are quite close to the overall thermal decomposition activation enthalpy determined by TGA of $\Delta H^{\ddagger}$ = 114.9 ± 3.6 kJ/mol. These products are identified to be CH_3NCS (73), methylimidazole (82), CH_3CH_2NCS (87), and ethylimidazole (96)[51] formed through an S_N2 type reaction, whereby the SCN^- anion attacks the alkyl groups on the imidazolium cation. This mechanism is further supported by VUV−PI−TOFMS appearance energies of these species in Table 3. Mass 142 will be discussed in the next section.

For BMIM$^+$DCA$^-$ and EMIM$^+$DCA$^-$, the major product masses detected were 82 and 97, and 82 and 96, respectively. While the 82 and 96 masses are likely methyl- and ethylimidazole formed via an S_N2 reaction similar to the thiocyanate ILs, the structure of mass 97 is not clear. A very small signal at m/z 124 was detected for BMIM$^+$DCA$^-$ that corresponds to the formation of butylimidazole, but the signal was too small to determine a thermal decomposition activation enthalpy for this species. The relatively small signal for butylimidazole is perhaps due to the lower vapor pressure of butylimidazole versus methyl- and ethylimidazole. For

dx.doi.org/10.1021/jp5095855 | J. Phys. Chem. A 2014, 118, 11119−11132

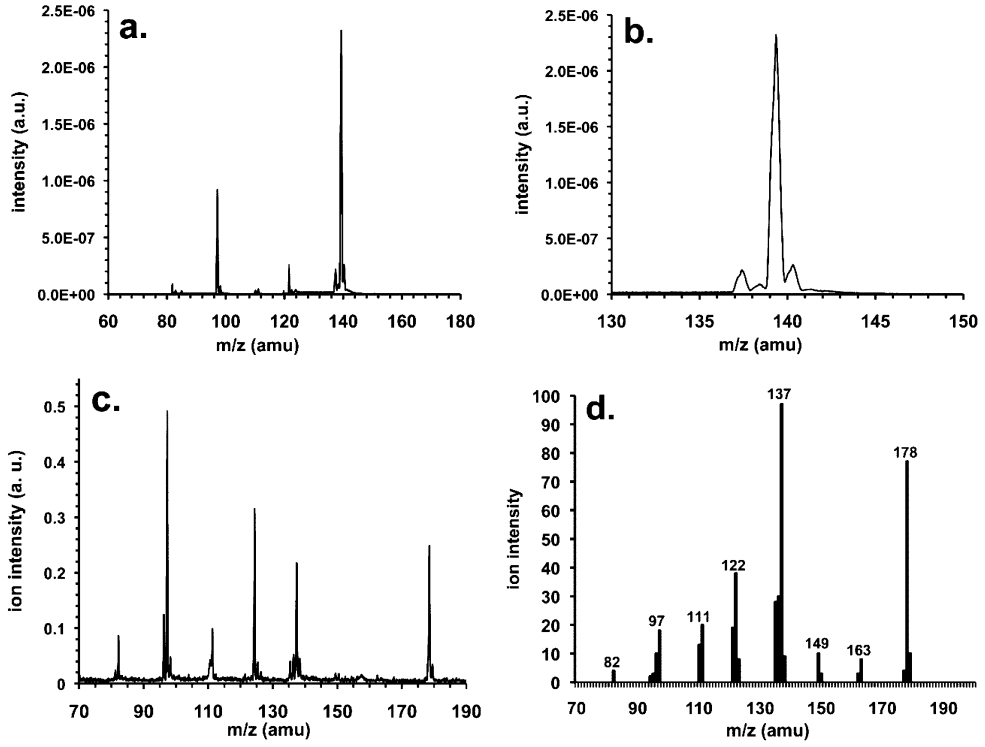

Figure 4. (a) VUV–PI–TOFMS spectrum of $BMIM^+DCA^-$ aerosol at 380 K and 10.0 eV and (b) expanded view of the $BMIM^+$ cation at m/z 139 from panel a, (c) $BMIM^+DCA^-$ spectrum from the effusive source at 483 K and 10.0 eV, and (d) GC–MS analysis of $BMIM^+DCA^-$ with 15 eV electron impact ionization energy.

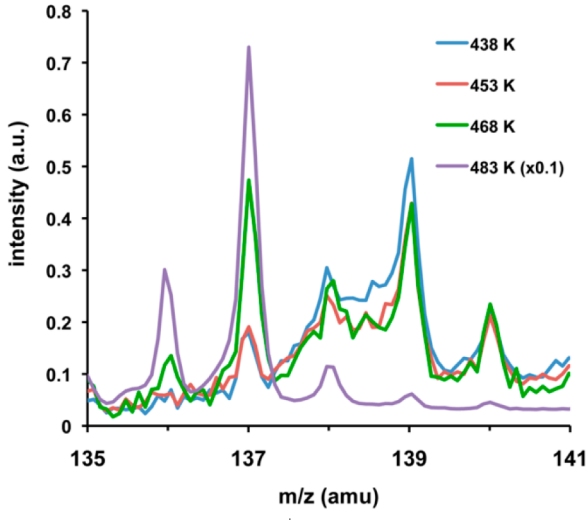

Figure 5. VUV–PI–TOFMS spectrum of $BMIM^+DCA^-$ for the effusive source in the range of 438–483 K at 12.0 eV photoionization energy, 5 million shots; traces are scaled for comparison.

$EMMIM^+DCA^-$, the primary masses detected were 110 and 96, corresponding to the S_N2 formation of 1-ethyl-2-methylimidazole and 1,2-dimethylimidazole.

Finally, for $BMIM^+TCM^-$, masses were detected via TGA–MS at 78, 82, 96, 107, and 124. While masses at m/z 82 and 124 are likely methylimidazole and butylimidazole, the sources of m/z 78, 96, and 107 are not clear, and further investigation is warranted.

C. Vacuum Ultraviolet Photoionization Time of Flight Mass Spectrometry. It is accepted that many aprotic ionic liquids evaporate as intact ion pairs: $C^+A^-(l) \rightarrow C^+A^-(g)$ and that upon ionization of these gaseous ion pairs, dissociation to the cation C^+ and the radical A is facile: $C^+A^- \rightarrow C^+A + e^- \rightarrow C^+ + A + e^-$.[8,9,52,53] Because of the very high detection sensitivity afforded at the Chemical Dynamics Beamline at the Advanced Light Source, the mass signals resulting from the ion pairs and those from thermal decomposition products or even trace contaminants or previous IL experiments needed to be carefully differentiated. In many cases, the thermal decomposition products are detected at lower source temperatures than, or simultaneously with, the ionic liquid vapors.

A common feature among the dialkylimidazolium ionic liquids investigated in this work was the significant loss of 1 amu from the $EMIM^+$ cations, loss of 2 amu from the $BMIM^+$ cations, and loss of 1 amu from the $EMMIM^+$ cation to a lesser extent. A second trend throughout the ionization of these ILs was the appearance of a mass peak in between the mass of the cation and the ion pair, namely, the mass of the (ion pair - 27) amu. Finally, as was mentioned previously, there is strong evidence of S_N2 dealkylation of the imidazolium by the anions. Previous work on ILs with more basic anions has determined that neutralization can occur through proton transfer from C2 on the imidazolium to the anion, leading to the formation of a neutral carbene[54,55] and an acid (protonated anion) which can then vaporize and be detected, unless the protonated anion can undergo polymerization to form a solid. In the case of $EMIM^+DCA^-$, the carbene is detected at m/z 110 with a photoionization energy of 7.6 ± 0.2 eV (Figure 3c) and matches well with the M06 calculated ionization energy for the EMIM carbene (EMIM:) of 7.7 ± 0.2 eV. While m/z 110 was not detected in the case of $EMIM^+SCN^-$, the formation of m/z 142 and HCN strongly suggest that these products are formed via the EMIM: carbene intermediate (Figure 7). The extent of carbene formation should be dependent on two factors: the

dx.doi.org/10.1021/jp5095855 | J. Phys. Chem. A 2014, 118, 11119–11132

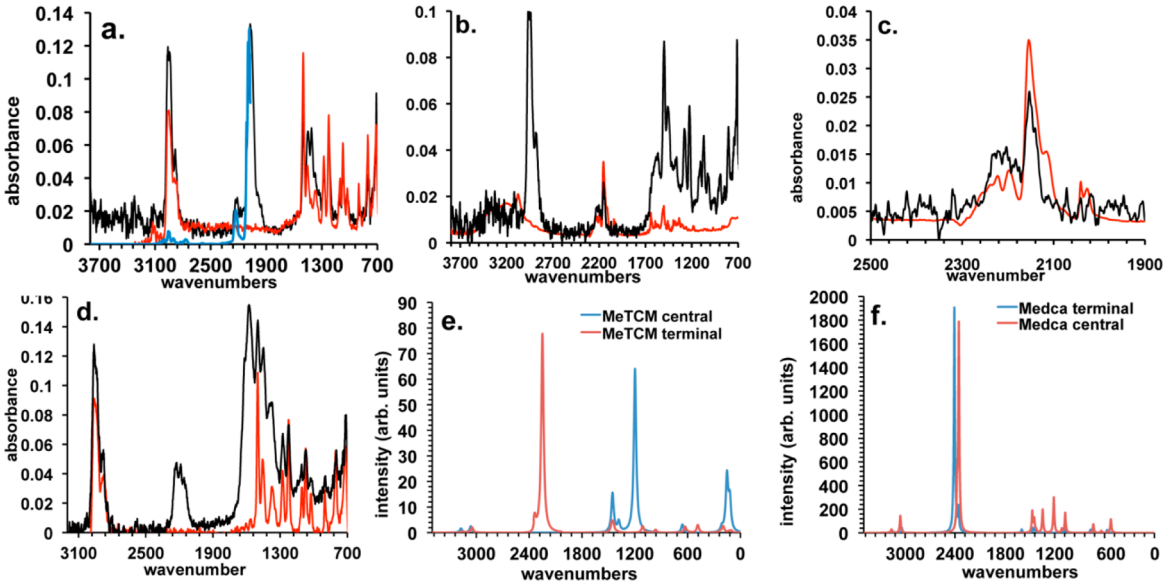

Figure 6. T-jump FTIR spectra of (a) $BMIM^+SCN^-$ decomposition products (black) compared to H_3CNCS (blue, ref 39) and 3:1 ratio of butylimidazole and methylimidazole (red), (b) $BMIM^+TCM^-$ decomposition products (black) and linear ketenimine (red, from ref 40), (c) an expanded view of the central peak in panel b, (d) $BMIM^+DCA^-$ decomposition products (black) and butylimidazole (red), (e) DFT IR simulation of methylated TCM^-, and (f) DFT IR simulation of methylated DCA^-.

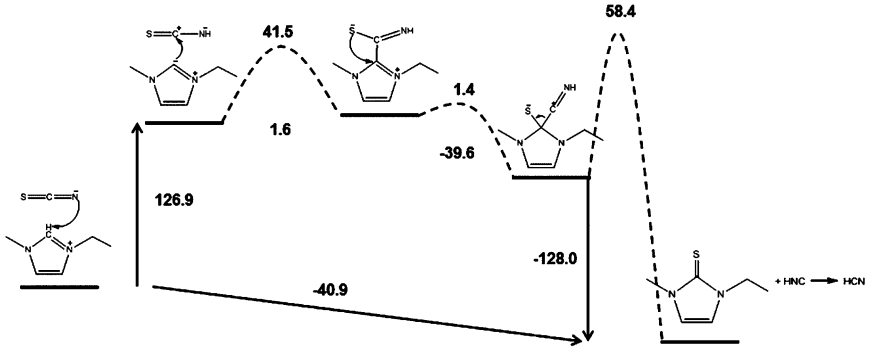

Figure 7. M06/6-31+G(d,p) free energy reaction profile of the thermal decomposition of $EMIM^+SCN^-$ leading to the formation of m/z 142 and HCN. Values are in kJ/mol.

Table 4. Calculated Free Energies of Acidity, ΔG_{acid}, in the Gas Phase and in the Condensed Phase, by SMD-GIL and SMD (water) at the M06/6-31+G(d,p) Level of Theory[a]

$\Delta G_{acid}(g)$		$\Delta G_{acid}(l)$		$\Delta G_{acid}(l)$	
acid	(kJ/mol)	acid	SMD-GIL (kJ/mol)	acid	SMD-H_2O (kJ/mol)
HNCS	1332.5	HNCS	607.0	HNCS	549.5
HNO_3	1306.7	HNCNCN	578.0	HNCNCN	521.8
HSCN	1274.2	HNO_3	566.6	HVDCA 04	515.2
HNCNCN	1272.6	HVDCA 01	565.2	HVDCA 01	514.6
NCNHCN	1234.6	HVDCA 04	564.9	NCNHCN	495.9
HVDCA 01	1212.1	NCNHCN	550.3	HNO_3	494.9
HVDCA 04	1203.3	HSCN	548.8	HSCN	492.6
HTCM (central)	1197.1	HTCM (central)	537.9	HTCM (centeral)	490.5
HTCM (terminal)	1188.7	HTCM (terminal)	533.9	HTCM (terminal)	483.9
HVDCA 02	1152.7	HVDCA 03	518.1	HVDCA 03	471.4
HVDCA 03	1146.1	HVDCA 02	517.6	HVDCA 02	468.6

[a]HVDCA 01 = terminal NH; HVDCA 02 = $-CCN_1H$; HVDCA 03 = $-CCN_2H$; HVDCA 04 = central NH.

basicity of the anion[2] and the stability of the carbene itself. Table 4 illustrates the relative strength of the base by determining the free energy of acidity: essentially how much free energy it takes to separate a proton from the acid HA. The higher the value of ΔG_{acid}, the more stable the acid HA and the less likely the anion will remain as a negative anion in the presence of acidic hydrogens. Species with $\Delta G_{acid}(g)$ values smaller than 300 kcal/mol (1255 kJ/mol) are considered to be

dx.doi.org/10.1021/jp5095855 | J. Phys. Chem. A 2014, 118, 11119−11132

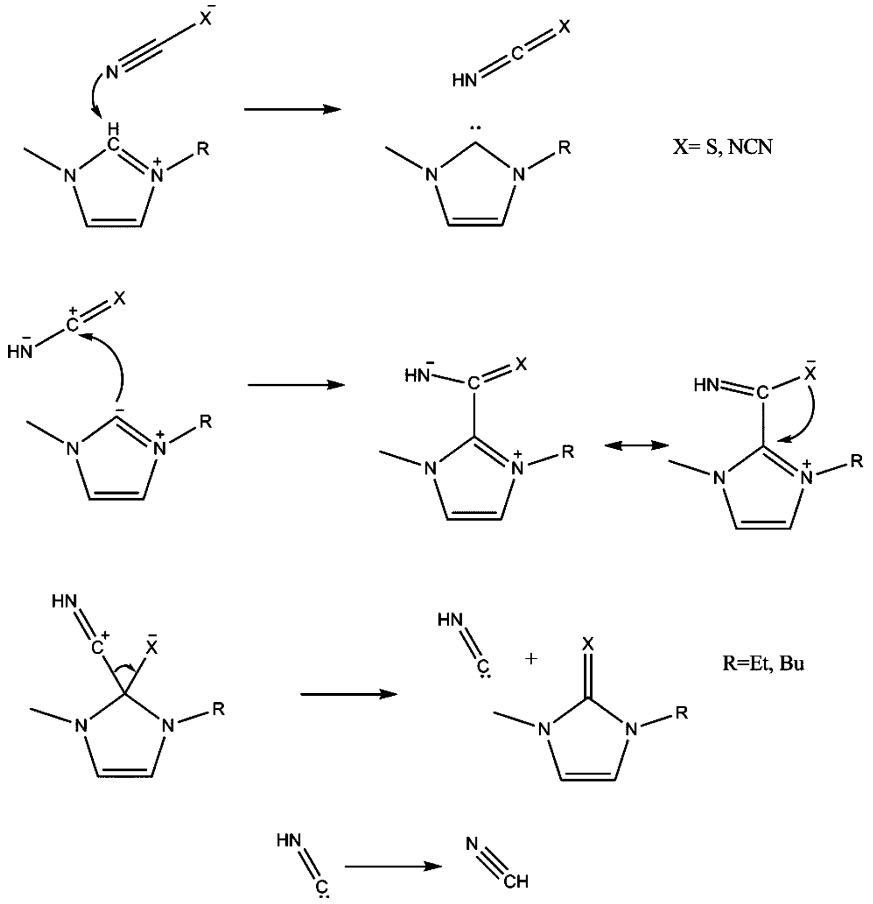

Figure 8. Generalized scheme for the addition−elimination reaction through a carbene intermediate.

superacids,[56] and these tend to make good candidates as anions for IL synthesis. The generic ionic liquid (SMD-GIL) variant[15] of the polarizable continuum model was employed here to calculate the $\Delta G_{acid}(l)$ values in an imidazolium ionic liquid and with water as a solvent as well (Table 4). The solvent effect on these systems reduces the free energy ΔG_{acid} values from around 1200 kJ/mol to around 520 kJ/mol in both the ionic liquid and in water. This reduction in energy is primarily driven by the large solvation energy of a proton (~550 kJ/mol) versus anions (~210 kJ/mol on average) in the condensed phases (Table in Supporting Information). On the basis of the ΔG_{acid} values in Table 4, the expected trend for formation of (C^+ - 1) amu photoions to appear in the VUV mass spectrum would be SCN^- > DCA^- > $VDCA^-$ > TCM^-. With the exception of $EMIM^+SCN^-$, which has a short-lived m/z 110 as described below, this trend is confirmed in the VUV experiments, and in fact, no (C^+ - 1) amu peak was detected for $BMIM^+TCM^-$. The ΔG_{acid} values for H^+ loss from the C2 of $EMIM^+$ and $BMIM^+$ or from the C2 methyl of $EMMIM^+$ are 262.9, 264.6, and 261.8 kJ/mol, respectively, and essentially are the same within the margin of error of M06, and therefore, the anion basicity is independent of cation for these cations. Note that the deprotonation of $EMMIM^+$ leads to formation of a stable methylene product at m/z 124 and not a reactive carbene species.[13]

The nitrate anion was included in this analysis to compare its relative basicity with the nitrile containing anions. Previous gas phase acidity calculations indicated that the DCA^- anion was less basic than the NO_3^- anion, and the equilibrium HNO_3 + DCA^- ↔ NO_3^- + HDCA would favor protonation of the NO_3^-.[4] From these SMD-GIL calculations, the solvation effect stabilizes HDCA more than HNO_3, and NO_3^- more than DCA^-, and would result in a spontaneous proton transfer from HNO_3 to DCA^-. Therefore, caution should be used in applying gas-phase ΔG_{acid} values to predict anion basicity. This solvation effect might help to explain the high reactivity of dicyanamide-based ionic liquids toward nitric acid.[4]

It is well-known that carbenes are highly reactive species,[54,55,57−59] and it is likely that these carbenes formed upon heating of the ILs are also involved in the formation of the species detected at m/z (C^+A^- - 27) amu seen in the DCA^-[22] and SCN^- systems. Additional evidence for these species was seen in the TGA−MS of $EMIM^+SCN^-$ (Supporting Information) and in the GC−MS trace of $BMIM^+DCA^-$ (Figure 4d), indicating that these products are thermodynamically stable. By determining the experimental VUV ionization potential (IP) of the m/z 27 photoion to be =13.4 ± 0.2 eV, this mass can be identified as HCN (I.P. = 13.4 eV[60]). Detailed ab initio analyses of the possible mechanisms of formation of m/z 142 + HCN from $EMIM^+SCN^-$ are shown in Figure 7. The proposed mechanism first involves the proton transfer to the SCN^- anion to form HNCS, which is more basic than HSCN (Table 4). This is followed by the rapid nucleophilic attack of the carbene at the carbon in HNCS. The nucleophilic attack by the carbene more likely occurs on the resonance-stabilized electropositive carbon (atomic charge = +0.112, M06/6-31+G(d,p)) than on the sulfur atom (atomic charge = +0.033, M06/6-31+G(d,p)). The S can then migrate to C2 on the imidazole ring, followed by HNC elimination from C2, which rapidly converts to HCN. This process

dx.doi.org/10.1021/jp5095855 | J. Phys. Chem. A 2014, 118, 11119−11132

effectively replaces the C2 proton in the ion pair with a sulfur atom, resulting in a neutral thioimidazole, which could explain the lack of m/z 110 for $EMIM^+SCN^-$ in the VUV−TOFMS spectra if the reaction is sufficiently fast once the carbene is formed. This scheme has been generalized to CN-containing anions in Figure 8. The more basic the anion is and, to a lesser extent, the more electrophilic the protonated anion is, the more likely this reaction is going to occur. These species are detected at temperatures slightly higher than the detection temperature of the carbenes, which is consistent with the small activation barrier involved in the nucleophilic attack of the carbene on the protonated anion (steps 2 to 3 in Figure 7). This type of mechanism may also explain the addition of an oxygen atom to the EMIM cation in the thermal decomposition of $EMIM^+NO_3^-$.[61] Although sulfur,[55] BF_3,[62,63] and PF_5[63] additions to C2 on the dialkylimidazolium cation through an *N*-heterocyclic carbene (NHC) intermediate have been demonstrated previously, to our knowledge, this is the first report of the NCN-ylidene being formed. Starting from the pure ionic liquid, this route could possibly be useful for a one-pot synthesis for these NCN imidazolium-ylidene species without the need for flammable solvents.

At even higher temperatures, the third major decomposition pathway indicated in the VUV−PI−TOFMS experiments is the S_N2 alkyl abstraction by the anion, as has been proposed previously[13,20,30,61,64] in ionic liquids. Because of steric constraints, the abstraction of the methyl group on the imidazolium cation is expected to be more facile than the bulkier ethyl or butyl groups, and this is evidenced by the lower activation energies for the formation of ethylimidazole or butylimidazole versus methylimidazole (Table 2 and supported by DFT calculations). Further evidence that this S_N2 reaction occurs is the detection of CH_3NCS and CH_3CH_2NCS in the thermal decomposition of $EMIM^+SCN^-$. The experimental IPs of mass 73 and 87 are 8.2 ± 0.2 and 9.1 ± 0.2 eV, respectively, while the M06 IP values are 9.1 ± 0.2 and 9.0 ± 0.2 eV for R−NCS (R=CH_3, CH_3CH_2−) and 9.9 ± 0.2 and 9.7 ± 0.2 eV for R−SCN (R=CH_3, CH_3CH_2−), giving a better match with the RNCS species. The temperature-jump experiments described below support this conclusion as well.

The appearance of the m/z 137 peak in the $BMIM^+$ ILs indicates that the $BMIM^+$ cation loses two hydrogens quite easily. It is possible that the mechanism for this involves the formation of the BMIM: carbene species, which could rapidly react to lose a second hydrogen. In Figure 5, the progression from the intact $BMIM^+$ cation (m/z 139, formed from dissociative photoionization of the vaporized ion pair) through the carbene (m/z 138) to m/z 137 as the temperature is raised from 438 to 483 K can be seen. At 438 and 453 K, the predominant peak is at m/z 139, with smaller peaks at m/z 138 and 137. At 468 K, the m/z 139 and 137 peaks are nearly equal in intensity, but the ratio of the m/z 139/138 peaks does not change significantly. This seems to indicate that if the m/z 137 species is formed via the BMIM: carbene (m/z 138), the carbene reacts quickly to form m/z 137 and is not detected. At 483 K, the m/z 139 peak nearly disappears and m/z 137 dominates, indicating that the rate of conversion of m/z 139 to 137 has surpassed evaporation, and the intensities of m/z 138 and 139 are consistent with ^{13}C isotopes resulting from the m/z 137 species. An interesting possibility is that the length of the butyl group allows the end of the butyl group to access the C2 carbene structure via rotations around the N−C and C−C bonds in the butyl group (see Scheme 1), whereas in the EMIM: the ethyl group is too short to react with the C2 carbene and does not lose a second hydrogen.

Scheme 1

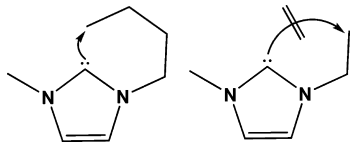

Bicyclic ionic liquids have been prepared from the BMIM cation-based ionic liquids,[65] which means that cyclization of the butyl group should be kinetically accessible to the BMIM carbene. It could be possible that m/z 137 is the result of conversion of the $BMIM^+$ cation to the bicyclic cation species (B^+, m/z 137) in the condensed phase through the carbene intermediate, which can then evaporate as a B^+A^- ion pair that undergoes dissociative photoionization to produce m/z 137 and $A^\bullet$. If the resulting B^+A^- has a lower enthalpy of vaporization than $BMIM^+A^-$ then the m/z 137 peak would dominate the mass spectrum versus m/z 139. Another possibility for the formation of m/z 137 is as an ionization fragment of m/z 178 (see GC−MS spectrum, Figure 4d). However, additional research is needed to understand and explain this phenomenon.

D. Temperature-Jump Fourier Transform Infrared Spectroscopy. In order to avoid polymerization reactions of the anions or alkylated anions, rapid heating to vaporize the thermal decomposition products prior to polymerization was performed using temperature-jump Fourier transform infrared spectroscopy. Additional evidence for the S_N2 alkyl abstractions is seen in the T-jump experiment involving $BMIM^+SCN^-$, which in Figure 6a clearly shows the formation of CH_3NCS. For $BMIM^+SCN^-$, the intense peak at 2080 cm^{-1} and smaller peak at ∼2200 cm^{-1} in Figure 6a suggests the formation of $SCN-CH_3$,[39] whereas $NCS-CH_3$ would have only a single peak at 2180 cm^{-1},[66] which is consistent with the VUV−PI−TOFMS results for $BMIM^+SCN^-$. Additional evidence for CH_3NCS formation is given by the m/z = 73 peak in the TGA−MS results. No HNCS or HSCN was detected. These experiments also indicate the demethylation of the imidazolium cation to form butylimidazole and a methylated anionic species for $BMIM^+TCM^-$ and $BMIM^+DCA^-$ ILs that were not detected in the TGA−MS or VUV−PI−TOFMS experiments. The methylated dicyanamide (with two −CN groups) and methylated tricyanomethanide (three −CN groups) products likely polymerize when heated slowly, which would explain their absence in the VUV−TOFMS and TGA−MS experiments, while methylated thiocyanate (with only one −CN group) cannot polymerize. For $BMIM^+TCM^-$, Figure 6b,c demonstrates a good match from 2100 to 2300 cm^{-1} with data from Finnerty et al.[40] (used with permission), indicating methylation of the terminal nitrogen on the tricyanomethanide species, $CH_3-NCC(CN)_2$, rather than at the central carbon, $CH_3-C(CN)_3$. This is consistent with the M06 IR simulation in Figure 6e indicating that there should be no peaks in this region for the centrally methylated species. For $BMIM^+DCA^-$ (Figure 6d), there are two peaks which arise from the methylated product at ∼1600 and ∼2200 cm^{-1}. From the M06 IR simulation (Figure 6f), both the terminally and centrally methylated dicyanamide species show peaks in the 2200 cm^{-1} range, so the identity of this product is not clear.

dx.doi.org/10.1021/jp5095855 | J. Phys. Chem. A 2014, 118, 11119−11132

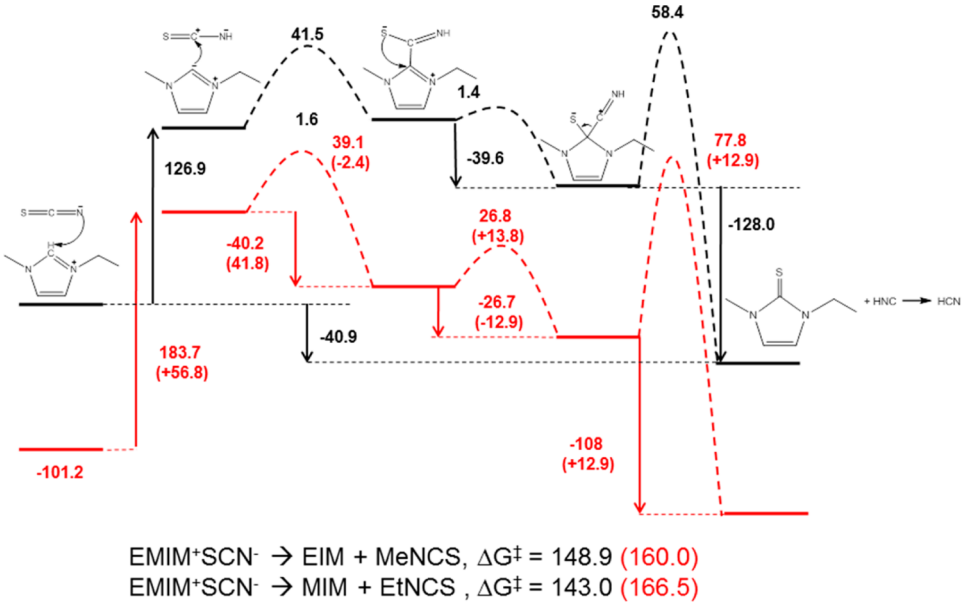

Figure 9. Free energy reaction profile comparison of gas phase (black) and SMD-GIL (red) using M06/6-31+G(d,p) for the formation of m/z 142 from $EMIM^+SCN^-$. Values are in kJ/mol.

However, the simulated spectrum of the terminally methylated species shows a small peak at ~1600 cm^{-1}, whereas the centrally methylated dicyanamide simulation does not show any peaks in this region. Also, previous DFT calculations indicate that the barrier to form the terminally methylated dicyanamide should be lower than for the centrally methylated product.[67]

E. Density Functional Theory Modeling. In order to verify the thermal decomposition mechanisms proposed based on the experimental evidence, hybrid density functional theory was applied at the M06/6-31+G(d,p) level of theory to these IL systems. M05 has been shown to provide a good level of theory for calculating energetics of ionic liquid systems (mean average deviation, MAD, of 9.5 kJ/mol),[24] and M06 is presumed to be as good if not better than M05 for our purposes. Stationary states of reactants, intermediates, transition states, and products, as well as adiabatic photoionization potentials were calculated. A representative free energy profile for $EMIM^+SCN^-$ is shown in Figure 7.

Adiabatic ionization potentials (IP) calculated for the proposed species match well with the experimentally determined photoionization energies (Table 3). For EMIM: (m/z 110), the experimentally determined value is 7.6 ± 0.2 eV and the M06 value is 7.7 ± 0.2 eV. Similarly, for the addition−elimination reactions (S, m/z 142 and 170, and −NCN: m/z 150 and 178 for $EMIM^+$ and $BMIM^+$, respectively, Figure 8), all of the experimental IPs match the M06 calculated IPs within 0.2 eV. In some cases, these species are detected at energies below the threshold to detect C^+ from dissociative ionization of the ion pair, which is an indication that these species are formed in the condensed phase and are not a result of dissociative photoionization.

F. Polarizable Continuum Model: SMD-GIL Method. In order to accurately represent the energetics involved in the liquid phase reactions of ionic liquids, a comparison was made between the gas phase $\Delta G_{acid}(g)$ calculations (Table 4) and the M06 energetics in Figure 7a and the corresponding energetics using the recent adaptation of the polarizable continuum model (PCM)[14] referred to as the generic ionic liquid (SMD-GIL) model.[15] This model parametrizes the PCM to accurately determine free energies of solvation and benchmarks to known experimental values, resulting in mean unsigned error (MUE) in free energy values of less than 1.85 kcal/mol. For $EMIM^+DCA^-$, the SMD-GIL solvent model has a MUE of 0.65 kcal/mol. For determining the $\Delta G_{acid}(l)$ in the condensed phase, the estimated error in these calculations is $\pm\sqrt{3} \times (0.65)$ kcal/mol or ±1.1 kcal/mol (±4.7 kJ/mol). The results for ΔG_{acid} are seen in Table 4.

The results of the SMD-GIL calculations for $EMIM^+SCN^-$ are seen in Figure 9. It is interesting to note that, relative to the gas phase, the free energy of solvation using the PCM model stabilizes the ion pair much more than the other neutral/molecular species and transition states, as has been observed previously in carboxylate ionic liquids.[13] Intuitively, this makes sense, as the ionic solvent will more readily solvate ions versus molecular species. The effect of lowering the free energy of the IL ion pair reactant more than the free energies of the intermediates, transition states, and products increases the initial free energy of activation in the condensed phase relative to the gas phase. Interestingly, the gas phase prediction of the activation barrier for the S_N2 reactions for $EMIM^+SCN^-$ incorrectly predicts the methyl abstraction to have a higher barrier than the ethyl abstraction, but the PCM model correctly predicts the methyl abstraction to be the more facile route.

G. Nucleophilicity of Anions. While nucleophilicity scales[68] are well-defined for many species in common solvents in which synthetic reactions are carried out (i.e., in H_2O, hexane, etc.), in the pure ionic liquids, the relative nucleophilicity of the nitrile containing anions toward alkyl abstraction from the dialkylimidazolium cations is not readily apparent. Even though extensive work has been performed to understand the nucleophilicity of anions in ionic liquids based on Kamlet−Taft β parameters,[2,69−74] these studies are based on solvent−solute interactions in either solvochromic shift experiments or in kinetics measurements of reactions where the IL acts as the solvent only and are therefore dependent on the nature of both the solvent and the solute. Disparities in the reported Kamlet−Taft parameters for ILs arise from the use of different solvochromic dyes and the presence of impurities in

dx.doi.org/10.1021/jp5095855 | J. Phys. Chem. A 2014, 118, 11119−11132

the IL.[69] Additionally, the Kamlet−Taft parameters' temperature dependence[75] has not been well characterized, and the trends predicted at 25 °C may not be applicable to thermal decomposition reactions at high temperature. In order to evaluate the nucleophilicity of these cyano-functionalized anions in the pure ILs, transition states of the S_N2 type methyl abstractions, the major alkyl abstraction reaction from the dialkylimidazolium cations (Scheme 2), were located in both

Scheme 2

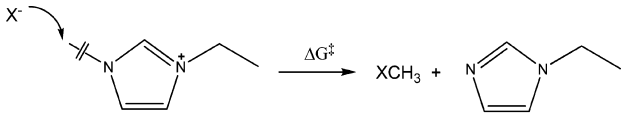

X = Br, SCN, dca, TCM

the gas phase and in the condensed phase using SMD-GIL to determine their free energies of activation (Table 5). The pathways with the lowest activation free energies would be expected to have the fastest alkyl abstraction rates and therefore be the most nucleophilic.[67,76] The free energies of activation for S_N2 methyl abstraction for SCN^-, DCA^-, TCM^-, and Br^- (for comparison to our previous study)[20] to form CH_3NCS, $CH_3N{=}C{=}NCN$, $CH_3N{=}C{=}C(CN)_2$, and CH_3Br, respectively, are seen in Table 5.

Table 5. Free Energies of Activation for S_N2 Methyl Abstraction from $EMIM^+$ by the Anion Calculated at the M06/6-31+G(d,p) Level of Theory and Using the Generic Ionic Liquid (GIL) Model to Simulate the Condensed Phase Methyl Abstraction

IL	$\Delta G^{\ddagger}$ (gas: M06) (kJ/mol)	$\Delta G^{\ddagger}$ (liquid: GIL) (kJ/mol)	$\Delta\Delta G$ (gas → liquid) (kJ/mol)
$EMIM^+Br^-$	138.6	134.6	−4.0
$EMIM^+DCA^-$	163.6	158.2	−5.4
$EMIM^+SCN^-$	148.9	160.0	11.1
$EMIM^+TCM^-$	175.8	181.5	5.7

From Table 5, the trend of relative nucleophilicities of the anions is, in decreasing nucleophilic strength: $Br^- > SCN^- > DCA^- > TCM^-$. It is interesting to note that the difference in the free energy of activation does not change significantly (from −4.0 to 11.1 kJ/mol) upon going from the M06 gas phase calculation to the GIL condensed phase calculation, which contrasts with the large shift in the free energy of activation for the initial proton transfer in the SCN^- system (Figure 9). Also, the trend for anion basicity and relative nucleophilicity are the same, but it is not apparent if this is coincidental or if this is a general trend. While the GIL model is an improvement over the gas phase approach to calculating the relative anion nucleophilicities proposed here, the gas phase calculations predict the same trend as the GIL method and could be considered a good first approximation to determining relative anion nucleophilicities in the pure ionic liquids.

VI. CONCLUSIONS

The thermal decomposition of alkylimidazolium ionic liquids with cyano-functionalized anions has been investigated by multiple, complementary experimental techniques and DFT CPCM (GIL) calculations. Two common thermal decomposition mechanisms have been confirmed, carbene formation and alkyl abstraction, which are related to anion basicity and nucleophilicity, respectively. Here we have proposed a third mechanism that likely proceeds through the carbene, which allows for addition of S or −NCN groups to C2 on the imidazole ring and could be useful for synthesis of substituted C2 imidazole synthesis. M06 calculations in the gas phase and the SMD-GIL variant of the polarizable continuum model for the condensed phase have demonstrated the ability to predict trends in anion basicity and anion nucleophilicity in pure ionic liquids, which should prove useful in predicting thermal stability trends in dialkylimidazolium ionic liquids and could be used as a higher accuracy method than the gas-phase DFT approach in predicting thermal stabilities of ionic liquids in general.

■ ASSOCIATED CONTENT

Supporting Information

Additional experimental data. This material is available free of charge via the Internet at http://pubs.acs.org.

■ AUTHOR INFORMATION

Corresponding Author

*E-mail: ghanshyam.vaghjiani@edwards.af.mil. Tel: 661-275-5657. Fax: 661-275-5471.

Notes

The authors declare no competing financial interest.

■ ACKNOWLEDGMENTS

We gratefully acknowledge the sample of $EMMIM^+DCA^-$ provided by Stefan Schneider and the GC−MS analysis performed by Amanda Wheaton at the Air Force Research Laboratory. S.D.C. gratefully acknowledges funding from the U.S. Air Force Office of Scientific Research (Grant No. FA9300-06-C-0023).

■ REFERENCES

(1) Ohno, H. *Bull. Chem. Soc. Jpn.* **2006**, *79*, 1665−1680.
(2) Crowhurst, L.; Mawdsley, P. R.; Perez-Arlandis, J. M.; Salter, P. A.; Welton, T. Solvent-Solute Interactions in Ionic Liquids. *Phys. Chem. Chem. Phys.* **2003**, *5*, 2790−2794.
(3) Schneider, S.; Hawkins, T.; Rosander, M.; Vaghjiani, G.; Chambreau, S.; Drake, G. Ionic Liquids as Hypergolic Fuels. *Energy Fuels* **2008**, *22*, 2871−2872.
(4) Chambreau, S. D.; Schneider, S.; Rosander, M.; Hawkins, T.; Gallegos, C. J.; Pastewait, M. F.; Vaghjiani, G. L. Fourier Transform Infrared Studies in Hypergolic Ignition of Ionic Liquids. *J. Phys. Chem. A* **2008**, *112*, 7816−7824.
(5) Earle, M. J.; Esperança, J. M. S. S.; Gilea, M. A.; Canongia Lopes, J. N.; Rebelo, L. P. N.; Magee, J. W.; Seddon, K. R.; Widegren, J. A. The Distillation and Volatility of Ionic Liquids. *Nature* **2006**, *439*, 831−834.
(6) Seeberger, A.; Andresen, A.-K.; Jess, A. Prediction of Long-Term Stability of Ionic Liquids at Elevated Temperatures by Means of Non-isothermal Thermogravimetrical Analysis. *Phys. Chem. Chem. Phys.* **2009**, *11*, 9375−9381.
(7) Zaitsau, D. H.; Kabo, G. J.; Strechan, A. A.; Paulechka, Y. U.; Tschersich, A.; Verevkin, S. P.; Heintz, A. Experimental Vapor Pressures of 1-Alkyl-3-methylimidazolium Bis-(trifluoromethylsulfonyl)imides and a Correlation Scheme for Estimation of Vaporization Enthalpies of Ionic Liquids. *J. Phys. Chem. A* **2006**, *110*, 7303−7306.
(8) Kelkar, M. S.; Maginn, E. J. Calculating the Enthalpy of Vaporization for Ionic Liquid Clusters. *J. Phys. Chem. B* **2007**, *111*, 9424−9427.

(9) Strasser, D.; Goulay, F.; Kelkar, M. S.; Maginn, E. J.; Leone, S. R. Photoelectron Spectrum of Isolated Ion-Pairs in Ionic Liquid Vapor. *J. Phys. Chem. A* **2007**, *111*, 3191−3915.
(10) Verevkin, S. P.; Zaitsau, D. H.; Emel'yanenko, V. N.; Yermalayeu, A. V.; Schick, C.; Liu, H.; Maginn, E. J.; Bulut, S.; Krossing, I.; Kalb, R. Making Sense of Enthalpy of Vaporization Trends for Ionic Liquids: New Experimental and Simulation Data Show a Simple Linear Relationship and Help Reconcile Previous Data. *J. Phys. Chem. B* **2013**, *117*, 6473−6486.
(11) Borodin, O.; Smith, G. D.; Kim, H. Viscosity of a Room Temperature Ionic Liquid: Predictions from Nonequilibrium and Equilibrium Molecular Dynamics Simulations. *J. Phys. Chem. B* **2009**, *113*, 4771−4774.
(12) Li, X.; Schatz, G. C.; Nesbitt, D. J. Anion Effects in the Scattering of CO_2 from the Room-Temperature Ionic Liquids [bmim][BF4] and [bmim][Tf2N]: Insights from Quantum Mechanics/Molecular Mechanics Trajectories. *J. Phys. Chem. B* **2012**, *116*, 3587−3602.
(13) Clough, M. T.; Geyer, K.; Hunt, P. A.; Mertes, J.; Welton, T. Thermal Decomposition of Carboxylate Ionic Liquids: Trends and Mechanisms. *Phys. Chem. Chem. Phys.* **2013**, *15*, 20480−20495.
(14) Tomasi, J.; Mannucci, B.; Cammi, R. Quantum Mechanical Continuum Solvation Models. *Chem. Rev.* **2005**, *105*, 2999−3093.
(15) Bernales, V. S.; Marenich, A. V.; Contreras, R.; Cramer, C. J.; Truhlar, D. G. Quantum Mechanical Continuum Solvation Models for Ionic Liquids. *J. Phys. Chem. B* **2012**, *116*, 9122−9129.
(16) Liu, J.; Chambreau, S. D.; Vaghjiani, G. L. Dynamics Simulations and Statistical Modeling of Thermal Decomposition of 1-Ethyl-3-methylimidazolium Dicyanamide and 1-Ethyl-2,3-dimethylimidazolium Dicyanamide. *J. Phys. Chem. A* **2014**, DOI: 10.1021/jp5095849.
(17) Maciejewski, J. P.; Gao, H.; Shreeve, J. M. Synthetic Methods for Preparing Ionic Liquids Containing Hypophosphite and Carbon-Extended Dicyanamide Anions. *Chem.—Eur. J.* **2013**, *19*, 2947−2950.
(18) Brill, T. B.; Brush, P. J.; James, K. J.; Shepherd, J. E.; Pfeiffer, K. J. T-Jump/FTIR Spectroscopy: a New Entry into the Rapid, Isothermal Pyrolysis Chemistry of Solids and Liquids. *Appl. Spectrosc.* **1992**, *46*, 900−911.
(19) Thynell, S. T.; Gongwer, P. E.; Brill, T. B. Condensed-Phase Kinetics of Cyclotrimethylenetrinitramine by Modeling the T-Jump/Infrared Spectrocopy Experiment. *J. Propul. Power* **1996**, *12*, 933−939.
(20) Chambreau, S. D.; Boatz, J. A.; Vaghjiani, G. L.; Koh, C.; Kostko, O.; Golan, A.; Leone, S. R. Thermal Decomposition of 1-Ethyl-3-methylimidazolium Bromide Ionic Liquid. *J. Phys. Chem. A* **2012**, *116*, 5867−5876.
(21) Chambreau, S. D.; Vaghjiani, G. L.; Koh, C.; Golan, A.; Leone, S. R. Ultraviolet Photoionization Efficiency of the Vaporized Ionic Liquid 1-Butyl-3-methylimidazolium Tricyanomethanide: Direct Detection of the Intact Ion Pair. *J. Phys. Chem. Lett.* **2012**, *3*, 2910−2914.
(22) Koh, C.; Liu, C.-L.; Harmon, C.; Strasser, D.; Golan, A.; Kostko, O.; Chambreau, S. D.; Vaghjiani, G. L.; Leone, S. R. Soft Ionization of Thermally Evaporated Hypergolic Ionic Liquid Aerosols. *J. Phys. Chem. A* **2011**, *115*, 4630−4635.
(23) Zhao, Y.; Truhlar, D. G. The M06 Suite of Density Functionals for Main Group Thermochemistry, Thermochemical Kinetics, Noncovalent Interactions, Excited States, and Transition Elements: Two New Functionals and Systematic Testing of Four M06-class Functionals and 12 Other Functionals. *Theor. Chem. Acc.* **2008**, *120*, 215−241.
(24) Izgorodina, E. I.; Bernard, U. L.; MacFarlane, D. R. Ion-Pair Binding Energies of Ionic Liquids: Can DFT Compete with Ab Initio-Based Methods? *J. Phys. Chem. A* **2009**, *113*, 7064−7072.
(25) Frisch, M. J.; Trucks, G. W.; Schlegel, H. B.; Scuseria, G. E.; Robb, M. A.; Cheeseman, J. R.; Scalmani, G.; Barone, V.; Mennucci, B.; Petersson, G. A.; et al. *Gaussian 09*, revision A.02; Gaussian, Inc.: Wallingford, CT, 2009.
(26) Marenich, A. V.; Cramer, C. J.; Truhlar, D. G. Universal Solvation Model Based on Solute Electron Density and on a Continuum Model of the Solvent Defined by the Bulk Dielectric Constant and Atomic Surface Tensions. *J. Phys. Chem. B* **2009**, *113*, 6378−6396.
(27) Heym, F.; Etzold, B. J. M.; Kern, C.; Jess, A. An Improved Method to Measure the Rate of Vaporisation and Thermal Decomposition of High Boiling Organic and Ionic Liquids by Thermogravimetrical Analysis. *Phys. Chem. Chem. Phys.* **2010**, *12*, 12089−12110.
(28) Luo, H.; Baker, G. A.; Dai, S. Isothermogravimetric Determination of the Enthalpies of Vaporization of 1-Alkyl-3-methylimidazolium Ionic Liquids. *J. Phys. Chem. B* **2008**, *112*, 10077−10081.
(29) Paulechka, Y. U.; Kabo, A. G.; Blokhin, A. V. Calorimetric Determination of the Enthalpy of 1-Butyl-3-methylimidazolium Bromide Synthesis: A Key Quantity in Thermodynamics of Ionic Liquids. *J. Chem. Phys. B* **2009**, *113*, 14742−14746.
(30) Lovelock, K. R. J.; Armstrong, J. P.; Licence, P.; Jones, R. G. Vaporisation and Thermal Decomposition of Dialkylimidazolium Halide Ion Ionic Liquids. *Phys. Chem. Chem. Phys.* **2014**, *16*, 1339−1353.
(31) Klomfar, J.; Souckova, M.; Patek, J. P-ρ-T Measurements for 1-Ethyl and 1-Butyl-3-Methylimidazolium Dicyanamides from Their Melting Temperature to 353K and up to 60 MPa in Pressure. *J. Chem. Eng. Data* **2012**, *57*, 1213−1221.
(32) Krolikowska, M.; Hofman, T. Densities, Isobaric Expansivities and Isothermal Compressibilities of the Thiocyanate-based Ionic Liquids at Temperatures (298.15−338.15 K) and Pressures up to 10 MPa. *Thermochim. Acta* **2012**, *530*, 1−6.
(33) Carvalho, P. J.; Regueira, T.; Santos, L. M. B. F.; Fernandez, J.; Coutinho, J. A. P. Effect of Water on the Viscosities and Densities of 1-Butyl-3-methylimidazolium Dicyanamide and 1-Butyl-3-methylimidazolium Tricyanomethane at Atmospheric Pressure. *J. Chem. Eng. Data* **2010**, *55*, 645−652.
(34) Gardas, R. L.; Freire, M. G.; Carvalho, P. J.; Marrucho, I. M.; Fonseca, I. M. A.; Ferreira, A. G. M.; Coutinho, J. A. P. P-ρ-T Measurements of Imidazolium-Based Ionic Liquids. *J. Chem. Eng. Data* **2007**, *52*, 1881−1888.
(35) Wooster, T. J.; Johanson, K. M.; Fraser, K. J.; MacFarlane, D. R.; Scott, J. L. Thermal Degradation of Cyano Containing Ionic Liquids. *Green Chem.* **2006**, *8*, 691−696.
(36) Chingin, K.; Perry, R. H.; Chambreau, S. D.; Vaghjiani, G. L.; Zare, R. N. Generation of Melamine Polymer Condensates upon Hypergolic Ignition of Dicyanamide Ionic Liquids. *Angew. Chem., Int. Ed.* **2011**, *50*, 8634−8637.
(37) Lotsch, B. V.; Schnick, W. Towards Novel C-N Materials: Crystal Structures of Two Polymorphs of Guanidinium Dicyanamide and Their Thermal Conversion into Melamine. *New J. Chem.* **2004**, *28*, 1129−1136.
(38) Chambreau, S. D.; Vaghjiani, G. L.; To, A.; Koh, C.; Strasser, D.; Kostko, O.; Leone, S. R. Heats of Vaporization of Room Temperature Ionic Liquids by Tunable Vacuum Ultraviolet Photoionization. *J. Phys. Chem. B* **2010**, *114*, 1361−1367.
(39) Johnson, T. J.; Sams, R. L.; Sharpe, S. W. The PNNL Quantitative Infrared Database for Gas-phase Sensing: a Spectral Library for Environmental, Hazmat, and Public Safety Standoff Detection. *Proceedings of SPIE 5269 Chemical and Biological Point Sensors for Homeland Defense*, Providence, RI, 2004.
(40) Finnerty, J.; Mitschke, U.; Wentrup, C. Linear Ketenimines. Variable Structures of C,C-Dicyanoketenimines and C,C-Bis-sulfonylketenimines. *J. Org. Chem.* **2002**, *67*, 1084−1092.
(41) Köddermann, T.; Paschek, D.; Ludwig, R. Ionic Liquids: Dissecting the Enthalpies of Vaporization. *ChemPhysChem* **2008**, *9*, 549−555.
(42) Swiderski, K.; McLean, A.; Gordon, C. M.; Vaughn, D. H. Estimates of Internal Energies of Vaporization of Some Room Temperature Ionic Liquids. *Chem. Commun.* **2004**, 2178−2179.
(43) Verevkin, S. P.; Emel'yanenko, V. N.; Zaitsau, D. H.; Heintz, A.; Muzny, C. D.; Frenkel, M. Thermochemistry of Imidazolium-Based Ionic Liquids: Experiment and First-Principles Calculations. *Phys. Chem. Chem. Phys.* **2010**, *12*, 14994−15000.

(44) Deyko, A.; Lovelock, K. R. J.; Corfield, J.-A.; Taylor, A. W.; Gooden, P. N.; Villar-Garcia, I. J.; Licence, P.; Jones, R. G.; Krasovskiy, V. G.; Chernikova, E. A.; et al. Measuring and Predicting $\Delta_{vap}H_{298}$ Values of Ionic Liquids. *Phys. Chem. Chem. Phys.* **2009**, *11*, 8544−8555.
(45) Emel'yanenko, V. N.; Verevkin, S. P.; Heintz, A. The Gaseous Enthalpy of Formation of the Ionic Liquid 1-Butyl-3-Methylimidazolium Dicyanamide from Combustion Calorimetry, Vapor Pressure Measurements, and Ab Initio Calculations. *J. Am. Chem. Soc.* **2007**, *129*, 3930−3937.
(46) Gross, J. H. Molecular Ions of Ionic Liquids in the Gas Phase. *J. Am. Soc. Mass Spectrom.* **2008**, *19*, 1347−1352.
(47) Trouton, F. On Molecular Latent Heat. *Philos. Mag., Ser. 5* **1884**, *18*, 54−57.
(48) Emel'yanenko, V. N.; Verevkin, S. P.; Heintz, A.; Corfield, J.-A.; Deyko, A.; Lovelock, K. R. J.; Licence, P.; Jones, R. G. Pyrrolidinium-Based Ionic Liquids. 1-Butyl-2-methyl Pyrroldinium Dicyanoamide: Thermochemical Measurement, Mass Spectrometry, and Ab Initio Calculations. *J. Phys. Chem. B* **2008**, *112*, 11734−11742.
(49) Emel'yanenko, V. N.; Zaitsau, D. H.; Verevkin, S. P.; Heintz, A.; Vos, K.; Schultz, A. Vaporization and Formation Enthalpies of 1-Alkyl-3-methyl-imidazolium Tricyanomethanides. *J. Phys. Chem. B* **2011**, *115*, 11712−11717.
(50) Fumino, K.; Wulf, A.; Verevkin, S. P.; Heintz, A.; Ludwig, R. Estimating Enthalpies of Vaporization of Imidazolium-Based Ionic Liquids from Far-Infrared Measurements. *ChemPhysChem* **2010**, *11*, 1623−1626.
(51) Stein, S. E. Mass Spectra. In *NIST Chemistry WebBook*; Linstrom, P. J., Mallard, W. G., Eds.; NIST Standard Reference Database Number 69; National Institute of Standards and Technology: Gaithersburg, MD; http://webbook.nist.gov.
(52) Armstrong, J. P.; Hurst, C.; Jones, R. G.; Licence, P.; Lovelock, K. R. J.; Satterly, C. J.; Villar-Garcia, I. J. Vapourisation of Ionic Liquids. *Phys. Chem. Chem. Phys.* **2007**, *9*, 982−990.
(53) Leal, J. P.; Esperança, J. M. S. S.; Minas da Piedade, M. E.; Canongia Lopes, J. N.; Rebelo, L. P. N.; Seddon, K. R. The Nature of Ionic Liquids in the Gas Phase. *J. Phys. Chem. A* **2007**, *111*, 6176−6182.
(54) Holloczki, O.; Gerhard, D.; Massone, K.; Szarvas, L.; Nemeth, B.; Veszpremi, T.; Nyulaszi, L. Carbenes in Ionic Liquids. *New J. Chem.* **2010**, *34*, 3004−3009.
(55) Rodriguez, H.; Gurau, G.; Holbrey, J. D.; Rogers, R. Reaction of Elemental Chalcogens with Imidazolium Acetates to Yield Imidazole-2-chalcogenones: Direct Evidence for Ionic Liquids as Proto-carbenes. *Chem. Commun.* **2011**, *47*, 3222−3224.
(56) Koppel, I. A.; Taft, R. W.; Anvia, F.; Hu, L.-Q.; Sung, K.-S.; DesMarteau, D. D.; Yagupolskii, L. M.; Yagupolskii, Y. L.; Ignat'ev, N. V.; Kondratenko, N. V.; et al. The Gas-Phase Acidities of Very Strong Neutral Bronstead Acids. *J. Am. Chem. Soc.* **1994**, *116*, 3047−3057.
(57) Arduengo, A. J.; Harlow, R. L.; Kline, M. A Stable Crystalline Carbene. *J. Am. Chem. Soc.* **1991**, *113*, 361−363.
(58) Igau, A.; Grutzmacher, H.; Baceiredo, A.; Bertrand, G. Analogous alpha, alpha'-Bis-Carbenoid Triply Bonded Species: Synthesis of a Stable λ3-phosphinocarbene-λ5-Phosphaacetylene. *J. Am. Chem. Soc.* **1988**, *110*, 6463−6466.
(59) Wanzlick, H. W.; Schonherr, H. J. Chemistry of Nucleophilic Carbenes. XVIII. 1,3,4,5-Tetraphenylimidazolium Perchlorate. *Liebigs Ann. Chem.* **1970**, *731*, 176−179.
(60) Lias, S. G. Ionization Energy Evaluation. In *NIST Chemistry WebBook*; Linstrom, P. J., Mallard, W. G., Eds.; NIST Standard Reference Database Number 69; National Institute of Standards and Technology: Gaithersburg, MD; http://webbook.nist.gov.
(61) Chowdhury, A.; Thynell, S. T. Confined Rapid Thermolysis/FTIR/ToF Studies of Imidazolium-based Ionic Liquids. *Thermochim. Acta* **2006**, *443*, 159−172.
(62) Taylor, A. W.; Lovelock, K. R. J.; Jones, R. G.; Licence, P. Borane-Substituted Imidazol-2-ylidenes: Syntheses in Vacuo. *Dalton Trans.* **2011**, *40*, 1463−1470.
(63) Tian, C.; Nie, W.; Borzov, M. V.; Su, P. High-Yield Thermolytic Conversion of Imidazolium Salts into Arduengo Carbene Adducts with BF_3 and PF_5. *Organometallics* **2012**, *31*, 1751−1760.
(64) Maton, C.; De Vos, N.; Stevens, C. V. Ionic Liquid Thermal Stabilities: Decomposition Mechanisms and Analysis Tools. *Chem. Soc. Rev.* **2013**, *42*, 5963−5977.
(65) Kan, H.-C.; Tseng, M.-C.; Chu, Y.-H. Bicyclic Imidazolium-based Ionic Liquids: Synthesis and Characterization. *Tetrahedron* **2007**, *63*, 1644−1653.
(66) Stein, S. E. Infrared Spectra. In *NIST Chemistry WebBook*; Linstrom, P. J., Mallard, W. G., Eds.; NIST Standard Reference Database Number 69; National Institute of Standards and Technology: Gaithersburg, MD; http://webbook.nist.gov.
(67) Kroon, M. C.; Buijs, W.; Peters, C. J.; Witkamp, G.-J. Quantum Chemical Aided Prediction of the Thermal Decomposition Mechanisms and Temperatures of Ionic Liquids. *Thermochim. Acta* **2007**, *465*, 40−47.
(68) Edwards, J. O. Correlation of Relative Rates and Equilibria with a Double Basicity Scale. *J. Am. Chem. Soc.* **1953**, *76*, 1540−1547.
(69) Ab Rani, M. A.; Brant, A.; Crowhurst, L.; Dolan, A.; Lui, M.; Hassan, N. H.; Hallett, J. P.; Hunt, P. A.; Niedermeyer, H.; Perez-Arlandis, J. M.; et al. Understanding the Polarity of Ionic Liquids. *Phys. Chem. Chem. Phys.* **2011**, *13*, 16831−16840.
(70) Bini, R.; Chiappe, C.; Mestre, V. L.; Pomelli, C. S.; Welton, T. A Rationalization of the Solvent Effect on the Diels-Alder Reaction in Ionic Liquids Using Multiparameter Linear Solvation Energy Relationships. *Org. Biomol. Chem.* **2008**, *6*, 2522−2529.
(71) Crowhurst, L.; Falcone, R.; Lancaster, N. L.; Llopis-Mestre, V.; Welton, T. Using Kamlet-Taft Solvent Descriptors To Explain the Reactivity of Anionic Nucleophiles in Ionic Liquids. *J. Org. Chem.* **2006**, *71*, 8847−8853.
(72) Fredlake, C. P.; Muldoon, M. J.; Aki, S. N. V. K.; Welton, T.; Brennecke, J. F. Solvent Strength of Ionic Liquid/CO_2 Mixtures. *Phys. Chem. Chem. Phys.* **2004**, *6*, 3280−3285.
(73) Lancaster, N. L.; Welton, T. Nucleophilicity in Ionic Liquids. 3.1 Anion Effects on Halide Nucleophilicity in a Series of 1-Butyl-3-methylimidazolium Ionic Liquids. *J. Org. Chem.* **2004**, *69*, 5986−5992.
(74) Ranieri, G.; Hallett, J. P.; Welton, T. Nucleophilic Reactions at Cationic Centers in Ionic Liquids and Molecular Solvents. *Ind. Eng. Chem. Res.* **2007**, *47*, 638−644.
(75) Trivedi, S.; Malek, N. I.; Behera, K.; Pandey, S. Temperature-Dependent Solvatochromic Probe Behavior within Ionic Liquids and (Ionic Liquid + Water) Mixtures. *J. Phys. Chem. B* **2010**, *114*, 8118−8125.
(76) Hao, Y.; Peng, J.; Hu, S.; Li, J.; Zhai, M. Thermal Decomposition of Allyl-Imidazolium-Based Ionic Liquid Studied by TGA-MS Analysis and DFT Calculations. *Thermochim. Acta* **2010**, *501*, 78−83.